









## Research Article

# Genetic Incorporation of Non-canonical Amino Acids in Anti-HER2 VHH: Expression and Characterization

Nuria Ramos<sup>1</sup>, Donna-Joe Bigot<sup>1</sup>, Gabrielle Zeder-Lutz<sup>2</sup>, Jean-Marc Strub<sup>3</sup>, Adilya Dagkesamanskaya<sup>1</sup>, Régis Fauré<sup>1</sup>, Sébastien Nouaille<sup>1</sup>, Cédric Y. Montanier<sup>1</sup>, Gilles Ferry<sup>4</sup>, Renaud Wagner<sup>2</sup>, Sarah Cianféran<sup>3</sup>, Jean Albert Boutin<sup>4\*</sup>, Gilles Truan<sup>1</sup>

<sup>1</sup>Toulouse Biotechnology Institute (TBI), Université de Toulouse, CNRS, INRAE, INSA, 31400 Toulouse, France

<sup>2</sup>Plateforme IMPReSS, UMR 7242, Biotechnologie et Signalisation Cellulaire, Ecole Supérieure de Biotechnologie de Strasbourg, 67412 Illkirch, France

<sup>3</sup>Laboratoire de Spectrométrie de Masse BioOrganique (LSMBO), Institut Pluridisciplinaire Hubert Curien – IPHC. CNRS UMR 7178, Université de Strasbourg, France and Infrastructure Nationale de Protéomique ProFI, FR2048 CNRS CEA, 67037 Strasbourg, France

<sup>4</sup>Pole d'expertise Biotechnologie, Chimie & Biologie, Institut de Recherches Servier, Croissy-sur-Seine, 78290 Croissy, France  
E-mail: ja.boutin.pro@gmail.com

**Received:** 28 November 2022; **Revised:** 24 February 2023; **Accepted:** 25 February 2023

**Abstract:** Nanobodies – or VHH – are small proteins (~120 residues) issued from antibodies with intact recognition for the original target of the antibody. In the present study, we show the possibility of incorporating non-canonical amino acids at precise locations of the sequence via classical genetic techniques (Genetic Code Expansion). We demonstrate that the amount of recombinant protein obtained is compatible with a large production format. We show that this protein can be purified, that its sequence corresponds to the theoretical molecular weight, and that the two non-canonical amino acids are incorporated at the desired locations of the sequence. Finally, we show by surface plasmon resonance (SPR) that the affinity of these VHHs is maintained towards their target, HER2.

**Keywords:** nanobodies, HER2, non-canonical amino acids, genetic incorporation, quality control, SPR

**Nonstandard abbreviations:** AzK is *N*<sup>ε</sup>-2-[(azidoethyloxy)carbonyl]-L-lysine; PrY is *O*-propargyl-L-tyrosine.

**Significance Statement:** Incorporation of non-canonical amino acids into an anti-HER2 VHH sequence is demonstrated step by step and leads to a VHH with similar characteristics to the wild-type VHH one.

## 1. Introduction

A change of paradigm has occurred in the last few years in the pharmaceutical industry. From mostly small molecule-oriented research on drug candidates, therapeutical research shifted to research based on biologics [1, 2]. Therapeutics tend to be mostly moving towards large molecular weight compounds, such as peptide or protein analogues [1], and going beyond this “simple” complexity to antibody-based [2] and cell-based (CAR-T cells [3])

---

Copyright ©2023 Nuria Ramos, et al.  
DOI: <https://doi.org/10.37256/nat.5120243482>  
This is an open-access article distributed under a CC BY license  
(Creative Commons Attribution 4.0 International License)  
<https://creativecommons.org/licenses/by/4.0/>

therapeutics, including engineered cells that are used in patient autotransfusion. The next steps in future therapy seem to be composed of engineered cells and self-produced vaccines as pandemic events push the limits of therapeutic solutions [4]. Those molecules were not considered anymore as providing substitutes for lacking, naturally produced proteins (such as insulin or growth hormones) but as potential drugs by themselves. Not only are the protein molecules constituted of naturally occurring amino acids, but more and more peptide-like structures (and beyond) comprise non-canonical amino acids. Reports showed such structures with capacities to act as drugs for human therapeutics. Furthermore, at almost the same time, a revolution occurred as antibodies could be used as human therapeutic agents.

The production of antibodies as agents for the therapeutic arsenal is dependent on novel approaches for their production, analyses, metabolic fate surveys, etc. Antibodies are “big” proteins of 150 kDa molecular weight. This huge change in mass (from small organic molecules of 300 Da average molecular weight) led to new fields of research, as we were looking for shorter versions of antibodies with intact antigen recognition in a much shorter version. Initially, the simplified antibodies from camels and sharks (see one of the first reviews of the subjects by Muyldermans et al. [5] and Clem et al. [6], respectively) were described. Then, the nanobodies – or single-domain heavy chain antibody fragments, VHH – came into play [7, 8].

It seems that a bias still exists in the use of VHHs. Indeed, one of the main uses of VHHs is as imaging agents [9–11]. The detection of the complex between the protein and the VHH, which is key in the imaging process, whether in diagnosis or in biochemical research, is the next difficulty to solve in order to have a “cheap” substitute for monoclonal antibodies. mAb can be detected with labeled secondary antibodies, but such tricks do not exist yet in the VHH domain. Due to the structure of the VHH and their lack of universal sequence against which one could develop secondary antibodies, the only way to reveal the VHH/target complex is to use labeled VHH. Several methods have been reported on how to obtain such labeled VHH. The main one is the introduction of a cysteine at the C-terminus and the subsequent selective introduction of a dye on this amino-acid prior to the formation of the VHH/target complex [12]. Another approach would be to fuse the VHH with a fluorescent protein, leading to a larger complex (VHH-GFP, for example) [13, 14]. One can also choose to label the VHH with radioactive atoms either in a positron emission tomography (PET) context (see Bao et al. [10] for review), or with iodine125 [15, 16] for traditional binding experiments that can lead to the quantification of the VHH/target complex. A third way that we also explored was to build a tetrameric VHH molecule that could be labeled on one of the VHH units [17].

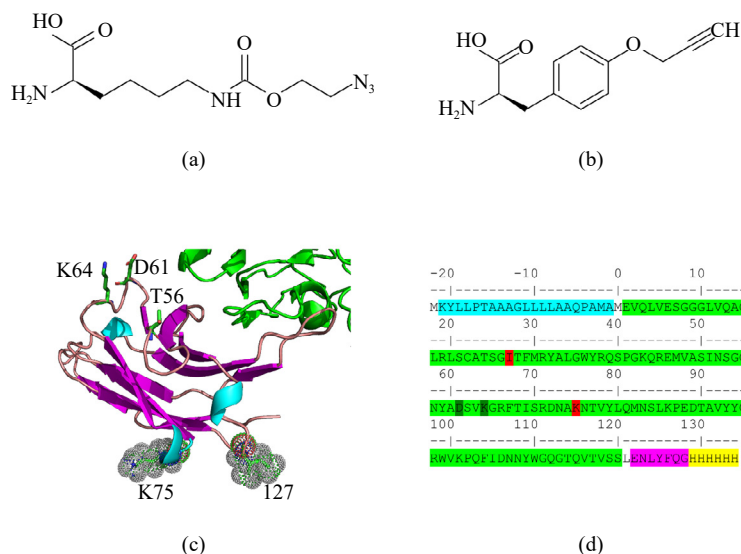
An alternative way is to introduce a handle in the sequence of the VHH. The handle can then be reacted, specifically by a click chemistry step in the ad hoc conditions, to subsequently attach a fluorophore to the handle. Such specific reactions can be performed via the incorporation of non-canonical amino acids (ncAAs) into specific locations in the VHH. In the last few years, a large body of literature has demonstrated the accessibility of incorporation techniques, notably via the Genetic Code Expansion technique [18–20]. These new trends are clearly reviewed and discussed by Gettemans and Dobbelaer [21]. Indeed, it is often necessary to covalently attach a specific reporter molecule to a location in the VHH sequence that does not impair or diminish the VHH’s capacity to recognize its “antigen”. Previous report(s) show that the integration of non-canonical amino acid(s) within the VHH sequence offers multiple advantages for the further use of those VHHs in research, diagnostic, or therapeutic purposes [22].

We report herein the full protocol for the production and purification of such modified VHHs. Three versions of VHH were produced and characterized. The present report shows that introducing ncAA at carefully identified places in the VHH sequence does not change the affinity of the final, mutant VHH vis-à-vis its “antigen” recognition.

## 2. Materials and methods

### 2.1 VHH samples

*N*<sup>ε</sup>-2-[(azidoethoxy)carbonyl]-L-lysine (AzK) and *O*-propargyl-L-tyrosine (PrY) were the selected non-canonical amino acids in the present report (see **Figures 1a and 1b** for structures). The wild-type (WT) form of the anti-HER2 VHH as well as all different mutants (I27AzK, I27PrY, T56Azk, T56PrY, D61AzK, D61PrY, K64AzK, K64PrY, K75AzK, K75PrY and the double mutant I27AzK + K75PrY, named dM1) were produced in *E. coli*. The WT sequence used was presented in our previous works [23, 24].



**Panels (a) and (b)** depict the structures of AzK ( $N^{\epsilon}$ -2-[(azidoethoxy)carbonyl]-L-lysine) and PrY (*O*-propargyl-L-tyrosine), respectively. **Panel (c)** represents a model of the anti-HER2 VHH (PDB 5MY6) with all 5 selected positions highlighted. The VHH is represented as a cartoon with cyan (alpha helices), magenta (beta sheets), and orange (loops), while HER2 is a green cartoon. T56, D61, and K64 are represented as green sticks with their respective labels, and I27 and K75 as dots with their respective labels too. **Panel (d)** shows the full sequence of the reconstructed VHH gene. In cyan, the pelB leader sequence; in green, the anti-HER2 sequence; in magenta, the TEV protease cleavage site; and in yellow, the His<sub>6</sub>-tag. The amino acids in red or dark green represent the positions (I27 and K75, wild-type VHH numbering) that were mutated to AzK and PrY, respectively.

**Figure 1.** Structures of the amino acids and wild-type and mutant anti-HER2 VHH

## 2.2 VHH plasmids and strains construction

The DNA fragments encoding the WT and mutant forms (stop codons at different positions in the coding sequence) of anti-HER2 VHH have been synthesized and cloned into the high copy expression vector pET-26b under the control of the T7 promoter. Poly(6)-His-tag and pelB leader sequences allowing for periplasmic localization were added at the protein C- and N-terminal ends, respectively (see **Figures 1c and 1d** for detailed sequences). The predicted spatial localizations of the ncAAs are shown in **Figure 1c**.

These genetic constructs were co-transformed into the *E. coli* strain *BL21(DE3)* with pEV10 plasmid, encoding for 2 aaRS/suppressor tRNA pairs: *Methanosarcina barkeri* pyrrolysyl-tRNA synthetase, *Methanosarcina mazei* pyrrolysyl-tRNA<sup>UUA</sup>opt (U25C) for the incorporation of AzK and *Methanocaldococcus janaschii* tyrosyl-tRNA synthetase mutant and tyrosyl-tRNA<sup>CUA</sup> for the incorporation of PrY. The expression of these two enzymes (induced by L-arabinose) and of the suppressor tRNAs is necessary for the incorporation of the ncAAs (AzK and PrF) in mutated proteins.

## 2.3 VHH bacterial expression

*E. coli* strains carrying two plasmids were cultured overnight in buffered TB medium with kanamycin A (20 mg/L) and chloramphenicol (30 mg/L). Cultures were diluted down to OD<sub>600</sub> = 0.05 in the same medium with 1 mM of each ncAA (final concentration) and grown at 28 °C until the OD<sub>600</sub> reached 0.6. At this point, aaRS and VHH expression were simultaneously induced by L-arabinose (at 0.02%, w/v) and IPTG (0.1 mM), and cultures were grown at 22 °C with vigorous shaking for 24 hours. Cells were then harvested by centrifugation (5,000 × g, 20 min, 4 °C), the supernatants were discarded, and the pellets were stored at -20 °C until further use.

## 2.4 VHH extraction and purification

Pellets from 50 mL of culture were resuspended in 2.5 mL of isosmotic buffer (10 mM Tris-HCl pH 8, 300 mM NaCl, 20% sucrose), incubated for 15 min on ice, then centrifuged at 6,000 × g for 10 min at 4 °C. The supernatant, containing the periplasmic proteins, was collected. The supernatant was loaded onto a Ni<sup>2+</sup>-NTA agarose (Qiagen) resin equilibrated with 20 mM Tris-HCl pH 8, 300 mM NaCl and 10 mM imidazole. The column was washed with the same

buffer containing 20 mM imidazole, and then the proteins were eluted with 250 mM imidazole. After dialysis of the sample against a phosphate-buffered saline (PBS) buffer, proteins were concentrated by centrifugation using an Amicon (Millipore) with a cutoff of 3 kDa.

## 2.5 SDS-PAGE and Western blot

Protein samples (10  $\mu$ L) were mixed with 1 volume of 2X SDS-PAGE loading buffer (0.15 M Tris-HCl pH 6.8, 10% mercaptoethanol, 1.2% SDS, 30% glycerol, 0.04% Bromophenol blue) and run on a 15% polyacrylamide SDS gel at 150 V for 1 hour. After the migration, gels were stained with InstantBlue™ (C.B.S. Scientific). Western blots were performed with an antibody against the 6-HisTag. Culture samples taken after an overnight IPTG induction were separated on the SDS-PAGE gel and transferred to the Immobilon-P membrane. The anti-6x-His Tag Monoclonal Antibody from Invitrogen was used to reveal the presence of the expressed proteins using the manufacturer's conditions.

## 2.6 Intact mass LC-MS analysis

Reverse phase LC-MS analysis was performed using an HP 1100 series (Agilent Technologies, Palo Alto, USA) coupled to a maXis II (BrukerDaltonics, Bremen, Germany) using a XBridge BEH300, C4, 3.5  $\mu$ m, 2.1 x 250 mm column (Waters, Milford, MA, USA) set at 60 °C. A gradient was generated (flow rate: 250  $\mu$ L/min) between phase A (aqueous with 0.1% trifluoroacetic acid [TFA]) and phase B (acetonitrile with 0.08% TFA). Mobile phase B was from 10 to 80% in 45 min, followed by a washing step of 5 min at 80% of phase B. Finally, an equilibrium period of 25 min was run in the starting conditions before the next injection. The maXis II instrument ran in positive mode under a capillary voltage of -4500 V. Acquisitions were performed in the mass range 300-3,000 m/z with a 1 s scan time. External mass calibration of the TOF was achieved before each set of analyses using Tuning Mix (Agilent Technologies) in the mass range of 322-2,722 m/z. Data analysis was performed by Compass DataAnalysis 4.3.110 software (Bruker).

Size exclusion chromatography (SEC) was performed on a BioAccord LC-MS system (Waters, Milford, MA, USA) equipped with an ACQUITY UPLC I-Class PLUS on a BEH SEC, 1.7  $\mu$ m, 2.1 x 250 mm column (Waters, Milford, MA, USA) set at 35 °C. The separation was performed at 100  $\mu$ L/min using a 150 mM ammonium acetate buffer at pH 6.9. The mass spectrometer was operated in positive mode with a mass range of 400-7,000 m/z. The capillary voltage was set at 1.5 kV, the cone voltage at 70 V, and the desolvation temperature was kept at 300 °C. The calibration was performed with Leucine Enkephalin compound for real-time mass correction.

## 2.7 Peptide mapping by nano LC-MS/MS

The liquid sample was submitted to reduction in the presence of 10 mM DTT in 25 mM  $\text{NH}_4\text{HCO}_3$  (1 h at 57 °C) and alkylation in the presence of 55 mM iodoacetamide in 25 mM  $\text{NH}_4\text{HCO}_3$ . The digestion was performed with a ratio E/S 1/20 with trypsin (12.5 ng/ $\mu$ L, Promega V5111) freshly diluted in 25 mM  $\text{NH}_4\text{HCO}_3$  and incubated overnight at 37 °C. The digested peptides were acidified by 0.1% HCOOH and analyzed by nano LC-MS/MS using a nanoACQUITY Ultra-Performance-LC (UPLC, Waters, Milford, MA) coupled to a Q-TOF (TripleTOF 5600+, Sciex) mass spectrometer. The samples were injected in a 20 x 0.18 mm, 5  $\mu$ m Symmetry C18 precolumn (Waters Corp.). The peptides were separated on a 75  $\mu$ m x 250 mm, 1.7  $\mu$ m particle size ACQUITY UPLC® BEH130 C18 column (Waters Corp.). The solvent system consisted of a solvent A (aqueous 0.1% formic acid) and solvent B (0.1% formic acid in acetonitrile). The trapping was performed for 3 min (5  $\mu$ L/min in 97% of A/3% of B). The elution was performed at a 300 nL/min flow rate, following a 3 to 40% solvent B gradient for 79 min, followed by 80% solvent B over 10 min at 60 °C. The MS and MS/MS analyses were performed on a hybrid quadrupole orthogonal acceleration time-of-flight tandem mass spectrometer, TripleTOF 5600 (Sciex). The instrument was set in positive mode, with settings as follows: ion spray voltage floating (ISVF) 2,300 V, curtain gas (CUR) 25 psi, interface heater temperature (IHT) 75 °C, ion source gas 1 (GS1) 2 psi, declustering potential (DP) 100 V. The acquisition mode (information-dependent acquisition; IDA) was used with the top 5 MS/MS scans. MS scans had accumulation times of 250 ms on the m/z (400-1,250) range, while the MS/MS scans were set at 100 ms and a m/z range of 150-1,600 in high sensitivity mode. The switching criteria were set for ions with charge states of 2-4 and an abundance threshold superior to 150 counts. The exclusion time was 12 s. The IDA rolling collision energy script was used for an automatic adaptation of the collision

energy (CE). The analyzer mass calibration was performed using peptides from digested bovine serum albumin. The system was completely controlled by the AnalystTF 1.6 software (AB Sciex). The peak list was searched using a SwissProt-derived combined target-decoy database (created 2020-12-14 and comprising the Homo sapiens 20,506 target sequences) and VHH sequence with and without modification(s) using the Mascot software (version 2.5.1, Matrix Science, London, England). During the database search, no enzyme was selected, and four variable modifications were included (that is, oxidation of Methionine [+16 Da], carbamidomethylation of Cysteine [+57 Da], AzK [+113 Da], PrY [+38 Da]). The peptide mass tolerance (for precursor ion measurements) was set to 15 ppm and the MS/MS mass tolerance (for fragment ion measurements) was set to 0.07 Da. Proline pipeline (<http://www.profi-proteomics.fr/proline/>) was used for the identification/validation of the results. The parameters for the validation of the peptide identification validation were as follows: a minimal length of seven amino acids, a score  $\geq 25$  and a pretty rank  $\leq 1$ .

## 2.8 Surface plasmon resonance (SPR) measurements

The experimental setup was as previously described [23] using a Biacore T200 instrument with the HER2 protein immobilized on sensor surfaces (CM5 sensorchips (BR100530), Cytiva) and the analyzed VHHs injected in a continuous flow over the surface.

### 2.8.1 HER2 protein immobilization

HER2 was immobilized with a standard amine coupling procedure [25] at a flow rate of  $10 \mu\text{L}\cdot\text{min}^{-1}$  in a running buffer (10 mM HEPES-pH 7.4, 150 mM NaCl, and 0.05% P20 surfactant). CM5 surfaces were activated by injecting a 1:1 mix of 0.2 M EDC [N-ethyl- N'-(3-dimethylaminopropyl)-carbodiimide hydrochloride] and 0.05 M NHS [N-hydroxy-succinimide] for 10 min. The his-tagged N-terminal extracellular domain of the human HER2 protein (Sino Biological, Cat. Number 10004-H08H) was diluted at 5 and  $25 \mu\text{g}\cdot\text{mL}^{-1}$  in acidic sodium acetate buffer (pH 5.5) and injected on two chip surfaces. After immobilization reached 180 RU and 5,000 RU, respectively, the remaining active groups were deactivated with 1 M ethanolamine hydrochloride at pH 8.5. A reference surface was treated similarly, omitting the HER2 injection.

### 2.8.2 Interaction experiments

The VHH samples were prepared in 50 mM Tris HCl at pH 7.5, 400 mM NaCl, and 0.05% P20 surfactant, which constitute the running buffer. Before the SPR experiments, the samples were centrifuged ( $17,000 \times g$ , 15 min,  $4^\circ\text{C}$ ), and the protein concentrations were measured spectrophotometrically (Nanodrop 2000) with the parameters Abs 0.1% (= 1 g/l) 1.92 and MW 14,024  $\text{g}\cdot\text{mol}^{-1}$ . All the samples and blanks were injected in duplicate. The HER2 surfaces were regenerated with two successive (10 s) injections of 2 M  $\text{MgCl}_2$ .

### 2.8.3 Concentration measurements

VHH concentrations were evaluated in the Calibration Free Concentration Analysis (CFCA) mode, with the VHHs (1 or 10 nM) injected for 60 s on both reference and high-density immobilized surfaces under flow rates of  $10 \mu\text{L}\cdot\text{min}^{-1}$  and  $80 \mu\text{L}\cdot\text{min}^{-1}$ . The dilution series were fitted using the CFCA functionality in Biacore T200 evaluation software v1. For the analyses, we used a diffusion coefficient of  $1.28 \times 10^{-10} \text{ m}^2/\text{s}$  and a VHH molecular weight of 14,024 Da. The validation criteria for the concentration measurements were those recommended by Biacore [26, 27].

### 2.8.4 Kinetic and affinity measurements

VHH samples at concentrations in the 0.5 to 30-45 nM (WT and K75 samples) or 1-150 or 430 nM (I27 and dM1 samples) ranges were serially injected for 300 s over reference and HER2 surfaces. Each VHH injection was followed by a 900 s buffer. The flow rate was  $50 \mu\text{L}\cdot\text{min}^{-1}$ .

### 2.8.5 Data analyses

The BIAevaluation T200 or the Scrubber 2.0c (BioLogic Software, Campbell, Australia) software was used for

SPR data processing. The sensorgrams were XY-zeroed prior to the injection start and were corrected for the signals recorded with the empty reference surface. The overlaid sensorgrams were processed by subtracting the average of the running buffer responses (double referencing [28, 29]). The protein concentration was determined from the binding data on the high-density HER2 surface using the CFCA evaluation feature of the BIAevaluation T200 software. The fitting procedure results in a globally determined concentration value, and the goodness of the fit is described by a  $\chi^2$  value that reaches a minimum, indicating that the reported value is robust [26]. The association ( $k_{on}$ ) and dissociation ( $k_{off}$ ) rate constants, the dissociation equilibrium constant ( $KD = k_{off}/k_{on}$ ), the maximum response (Rmax) were determined using a simple 1:1 Langmuir interaction model by regression analysis. The fitting procedure results in globally determined kinetic parameters and Rmax values, and the goodness of the fit is described by a  $\chi^2$  value.

## 3. Results

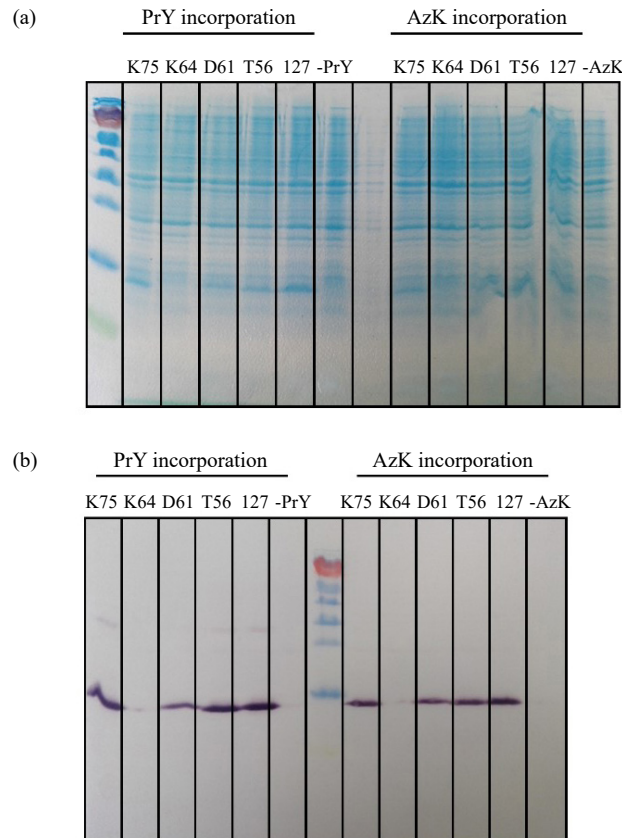
### 3.1 Selection of the targeted positions on the VHH

We targeted the standard anti-HER2 VHH that we explored before [17, 23, 24] in order to compare and ease our understanding of the production systems. We chose two ncAAs as models for this approach, namely  $N^{\epsilon}$ -2-[(azidoethoxy)carbonyl]-L-lysine (AzK) and *O*-propargyl-L-tyrosine (PrY), mostly because the incorporation of these two ncAAs has been widely described [19, 30, 31]. The locations in which ncAAs were incorporated were carefully chosen based on the positions of the residues to be changed in the three-dimensional structure of the VHH/HER2 crystal complex (**Figure 1c**). All five selected positions (I27, T56, D61, K64, and K75; see **Figure 1c** for their location on the structure of the VHH and **Figure 1d** for their positions in the full sequence of the VHH) are located on the surface of the VHH, all at a minimum of 6.0 Å distance from the closest sidechain of HER2, thus limiting the possible collapse of affinity between the ncAA-bearing VHH and its antigen.

### 3.2 Preliminary steps of expression

Sequences bearing the amber codon at various positions (27, 56, 61, 64, and 75; see **Figure 1d** for the VHH sequence) were built. All positions were tested with either PrY or AzK incorporation (**Figure 2**). Without the ncAA (-PrK or -AzK lanes), no expression was detectable, either by SDS-PAGE analysis or western blot, as the truncated product is small and does not contain the Poly His<sub>6</sub>-Tag that is used as an antigen for the primary antibody binding. Evaluation of the yield of incorporation was performed with small volume cultures, in the presence or absence of each ncAA and further analyzed via SDS-PAGE of the full extract (**Figure 2a**) or a western blot (**Figure 2b**) with an antibody directed against the Poly His<sub>6</sub>-Tag. Among all tested positions, PrY is slightly better incorporated than AzK. Among all tested positions, only one (K64) could not show any incorporation of either PrY or AzK. D61 and T56 showed incorporation of both ncAAs, however, I27 and K75 demonstrate better incorporation with Prk and AzK. The relative positions of the two latter residues on the structure (**Figure 1c**) do not reveal any particular feature compared to the other three: all of them are on the surface, either on loops or secondary structures. We therefore selected I27 and K75 for purification and characterization of the VHH with one or two incorporated ncAAs.





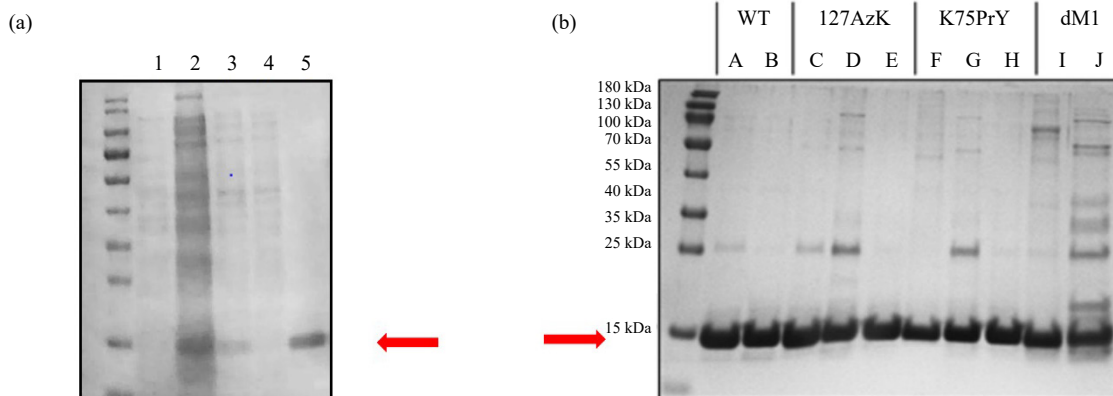
The tests for expression were performed after transformation of *E. coli* strain BL21(DE3) with pET-26b bearing the mutated VHH and pEV10 containing the tRNA synthetases and tRNA for the 5 possible positions of mutations selected from Figure 1c (namely, T56, D61, K64, 127, and K75). **Panel (a)**: SDS-PAGE analysis of the five *E. coli* full extracts with PrK or AzK in the culture medium. The Thermo Scientific™ PageRuler™ Prestained Protein Ladder is deposited in the first lane. The last lane for each set corresponds to the expression of 127 without ncAA (PrY or AzK). The red box points out the region where the VHH protein is expected. **Panel (b)**: Western Blot of the same samples. The primary antibody is directed against the Poly His<sub>6</sub>-Tag. The Thermo Scientific™ PageRuler™ Prestained Protein Ladder is deposited in the middle lane.

**Figure 2.** Analysis of the expression level of the five mutants with both ncAAs

### 3.3 Expression and purification processes

The VHH were produced as described, with slight modifications from our previous protocols [23, 24, 32]. The end products were four proteins purified to almost homogeneity by immobilized metal affinity chromatography (IMAC), thanks to the C-terminal His<sub>6</sub>-Tag. The final products, as can be seen from **Figure 3a, lane 5, and Figure 3b**, were essentially pure even when the double-mutant (dM1) was expressed. **Figure 3b** shows several independent productions, with a major band in the 15 kDa area, ensuring the predominance of the VHH protein. Note that in some preparations (**Figure 3b, lanes D and G**), a contaminant appears at twice the molecular weight value, suggesting dimerization. In lane I, the very high molecular weight might be a polymer of the VHH, a pattern already detected in previous experiments with the WT anti-HER2 VHH [17].

The purity of the preparations was evaluated to be superior to 95%. This material was used for the precise evaluation of the sequences of the VHH mutants and the incorporation of the ncAAs.



**Panel (a):** Example of the purification process of a mutated VHH bearing a ncAA. **Lane 1:** Bacterial culture before IPTG induction of the expression of the VHH; **Lane 2:** Bacterial culture after 24 hours of induction; **Lane 3:** periplasmic expression of the VHH; **Lane 4:** Flow-through onto the Ni affinity column; **Lane 5:** final elution by imidazole before concentration. **Panel (b):** Samples taken from different expression/purification steps of the various anti-HER2 VHH were analyzed by SDS-PAGE in standard conditions. The red arrow shows the protein of interest. Lanes A and B: **WT:** wild-type anti-HER2 VHH; Lanes C, D, and E: **I27AzK:** Mutated VHH bearing AzK at position 27; Lanes C, D, and E: **K75PrY:** mutated VHH bearing PrY at position 75; Lanes F, G, and H: **dM1:** doubly mutated VHH bearing both ncAAs at positions 27 and 75.

**Figure 3.** SDS-PAGE analysis of the produced VHH

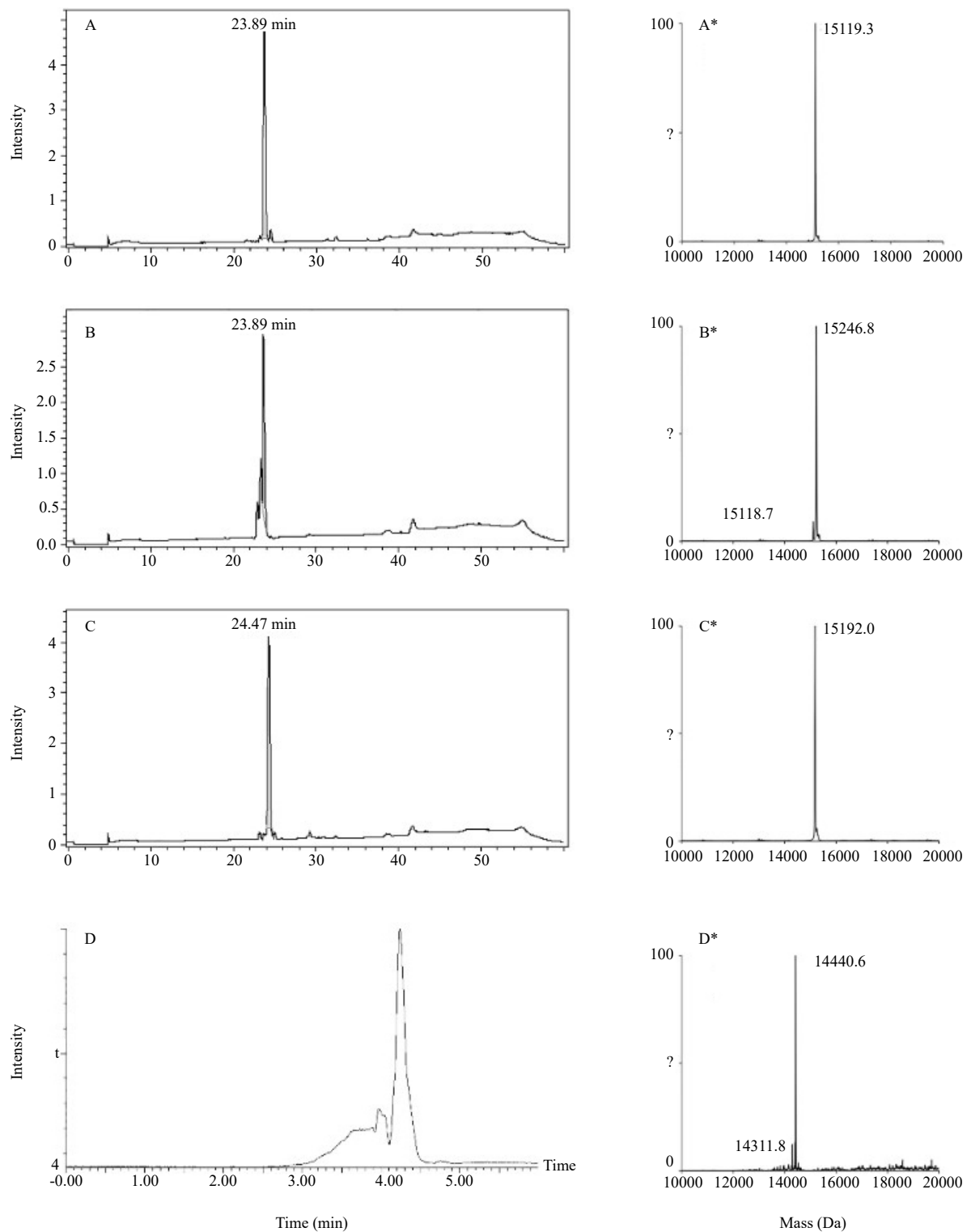
The intact mass measurements indicate the complete cleavage of the pelB leader sequence signal peptide and the presence of the N-terminus methionine residue, as well as the formation of one disulfide bridge between the two available cysteine residues for WT VHH and for VHH mutants **K75PrY** and **I27AzK**, which demonstrates that ncAAs have been successfully integrated in the VHH sequences. These VHHs (WT and mutants **K75PrY** or **I27AzK**) span from Met<sup>0</sup> to His<sup>134</sup>. Of note, a minor population (8%) of WT-VHH that has not incorporated the ncAA was also detected in the mutant **I27AzK** preparations. Similarly, the **dM1** mutant incorporated both ncAAs, but with some consequences. The proteomic analysis of the **dM1** mutant highlighted two different masses, corresponding to different sequences, with the protein spanning from either Met<sup>0</sup> to the Gln<sup>127</sup> (14440.2 Da) or Glu<sup>1</sup> to the Gln<sup>127</sup> (14311.8 Da; see **Figure 1a** for sequences). These modifications translate into a loss of nine amino acids at the C-terminus and the addition of three at the N-terminus, signing a proteolysis in the last steps of the purifications, certainly due to the configuration changes resulting from the introduction of both ncAAs. These VHHs span from Met<sup>0</sup> to His<sup>134</sup>. Similarly, the **dM1** mutant incorporated both ncAAs, but with some consequences. The proteomic analysis of the **dM1** mutant could not detect any other protein but **dM1**, although the protein spans from Ala<sup>-3</sup> to Tyr<sup>125</sup>. Thus, the corresponding mass, 14440.2 Da, corresponds to the proteins from AMAME at the N-terminus and finishing at LENLY, at the C-terminus, as expected (see **Figure 1a** for sequences). This modification in mass and sequence translates into a loss of nine amino acids at the C-terminus and the addition of three at the N-terminus, signing a proteolysis in the last steps of the purifications, certainly due to the configuration changes resulting from the introduction of both ncAAs.

Peptide mass fingerprints allowed demonstrating that the ncAAs were inserted at the correct position. Indeed, the next set of analyses shows the exact localization of the incorporations of the ncAAs into the sequence, either in the monomodified VHHs (**Figures 5A and 5B**) or in the double mutant (**Figures 5C and 5D**). In conclusion, our results highlight the correct insertion of a single ncAA for the single mutants **I27AzK** and **K75PrY** and of two ncAA for the double mutant **dM1**, at the desired positions, as shown from the mass spectrometry analyses.

### 3.4 Mass spectrometry analyses

The C-terminal location of the Poly His<sub>6</sub>-Tag for the WT and mutant proteins, as well as the size of the bands corresponding to a full-length VHH, indicated that the translation continued after the stop codons introduced for ncAA incorporation. Nonetheless, we wanted to further verify (i) that the whole proteins were readily and exactly expressed and (ii) that the ncAAs incorporated were intact and at the predicted positions. To do so, we performed intact mass analysis of the different VHH by either LC/MS in denaturing conditions for WT VHH, VHH mutant **K75PrY**, and **I27Azk**, or by SEC-MS in native conditions for VHH **dM1**, as shown in **Figure 4**. The results of the mass measurement of the main chromatographic peaks for WT VHH and mutants are presented in **Table 1**.





Reversed-phase LC-MS analysis of WT VHH (A), VHH mutants **I27AzK** (B), and **K75PrY** (C). Size exclusion chromatography LC-MS analysis in native conditions of the VHH double mutant dM1 (D). Figures A, B, C, and D present the total ion current of WT VHH (A), VHH mutants I27AzK (B), VHH mutants K75PrY (C), and VHH double mutant dM1 (D). The figures A\*, B\*, C\*, and D\* present the deconvoluted mass spectra of WT VHH (A\*), VHH mutants **I27AzK** (B\*), VHH mutants **K75PrY** (C\*), and VHH double mutant dM1 (D\*).

**Figure 4.** LC-MS analyses of the WT and mutated VHHs

**Table 1.** Theoretical and experimental masses of the four VHHs

Sample	Calculated average mass	Measured average mass	Error in Da	Interpretation
A	15118.9	15119.3	0.4	VHH-wt 0-134
	15246.9	15246.8	0.1	VHH-I27 0-134
B	15118.9	15118.7	0.2	VHH-wt 0-134
	15191.9	15192	0.1	VHH-K75 0-134
C	14440.2	14440.6	0.4	VHH-I27-K75 0-127
	14311.0	14311.8	0.8	VHH-I27-K75 1-127

**Sequence A: VHH-WT**

M<sub>0</sub>EVQLVESGG GLVQAGGSLR LSCATSGITF MRYALGWYRQ SPGKQREMVA SINSGGTTNY ADSVKGRFTI SRD<sub>N</sub>AKNTVY LQMNSLKPED TAVYYCNARW VKPQFIDNNY WGQGTQVTVS SLENLYFQGH HHHHH<sub>134</sub>

**Sequence B: VHH mutants I27AzK**

M<sub>0</sub>EVQLVESGG GLVQAGGSLR LSCATSGK<sup>Az</sup>TF MRYALGWYRQ SPGKQREMVA SINSGGTTNY ADSVKGRFTI SRD<sub>N</sub>AKNTVY LQMNSLKPED TAVYYCNARW VKPQFIDNNY WGQGTQVTVS SLENLYFQGH HHHHH<sub>134</sub>

**Sequence C: VHH mutants K75PrY**

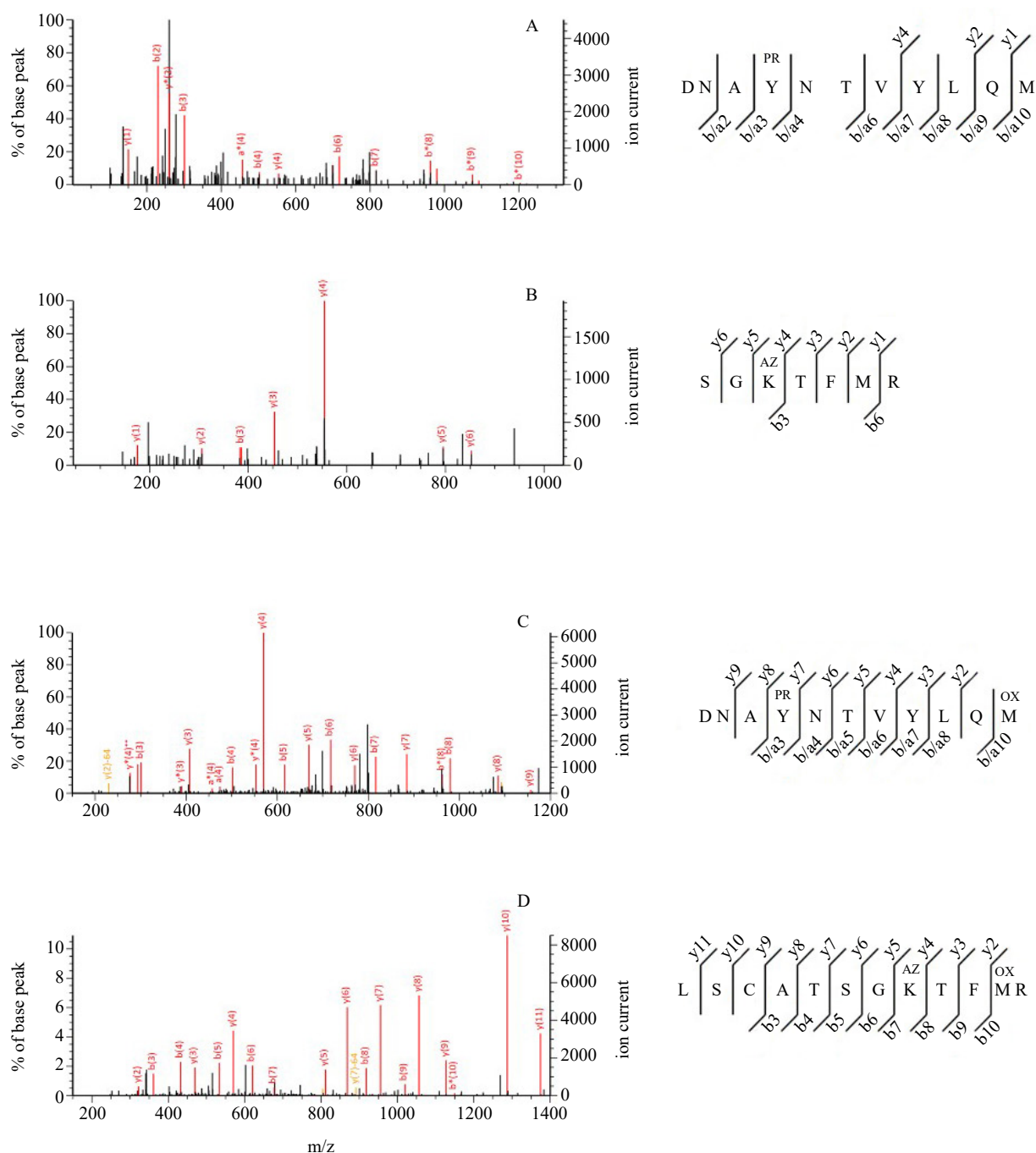
M<sub>0</sub>EVQLVESGG GLVQAGGSLR LSCATSGBTF MRYALGWYRQ SPGKQREMVA SINSGGTTNY ADSVKGRFTI SRD<sub>N</sub>AY<sup>Pr</sup>NTVY LQMNSLKPED TAVYYCNARW VKPQFIDNNY WGQGTQVTVS SLENLYFQGH HHHHH<sub>134</sub>

**Sequence D: VHH double mutant dM1**

M<sub>0</sub>E1VQLVESGG GLVQAGGSLR LSCATSGK<sup>Az</sup>TF M RYALGWYRQ SPGKQREMVA SINSGGTTNY ADSVKGRFTI SRD<sub>N</sub>AY<sup>Pr</sup>NTVY LQMNSLKPED TAVYYCNARW VKPQFIDNNY WGQGTQVTVS SLENLYFQ<sub>127</sub>GH HHHHH

K<sup>Az</sup> is N<sup>ε</sup>-2-[(azidoethoxy)carbonyl]-L-lysine and Y<sup>Pr</sup> is O-propargyl-L-tyrosine

This table contains the calculated and the measured masses of the four different forms of VHH and the interpretation of the masses detected in **Figure 4**. The presence of one disulfide bridge is taken into account for the mass calculation.



**Panel A:** MS/MS mass spectrum of the peptide DNAYPrNTVYLQM with a propargyl-tyrosine in position 75 ( $Y^{Pr}$ ) on VHH mutant K75. **Panel B:** MS/MS mass spectrum of the peptide SGKAZTFMR with an azido-lysine in position 27 ( $K^{Az}$ ) on VHH mutant I27. **Panel C:** MS/MS mass spectrum of the peptide DNAY<sup>Pr</sup>NTVYLQM with a propargyl-tyrosine in position 75 ( $Y^{Pr}$ ) on the VHH double mutant. **Panel D:** MS/MS mass spectrum of the peptide LSCATSG KAZ TFMR with an azido-lysine in position 27 ( $K^{Az}$ ) on the double mutant.

**Figure 5.** Detailed MS/MS spectra showing the incorporation of the non-canonical amino acids

### 3.5 SPR data

The binding capacity of VHH samples to the immobilized C-terminal part of the HER2 protein was assessed. We first determined the active concentration of each VHH batch by measuring its ability to bind to the HER2 epitope, which is not necessarily identical to the total concentration as measured by spectrophotometry.

#### 3.5.1 Measurement of active concentration of the VHH samples

The percentage of active VHH determined by Calibration-Free Concentration Analysis (**Figure 6**), exceeded 65% of the soluble fraction for the VHH sources but was lower (~40%) for the VHH-I27-K75 sample (**Table 2**). The higher active concentration determined for VHH WT determined by SPR (155%) could be explained by an underestimation of the total concentration measured by spectrometry at 280 nm or by dilution uncertainty. The concentration assessed by CFCA may also be subject to an error factor of 15-30% under some conditions [27]. The sensorgrams of the VHH WT/HER2 interaction are consistent with the mass transport limitation required to measure accurate active concentration by SPR, i.e., the binding rates clearly depend on the flow rates, showing a high QC ratio (0.877; **Figure 6A**), and the concentration is measured from the direct fitting of the slopes.

### 3.6 General considerations

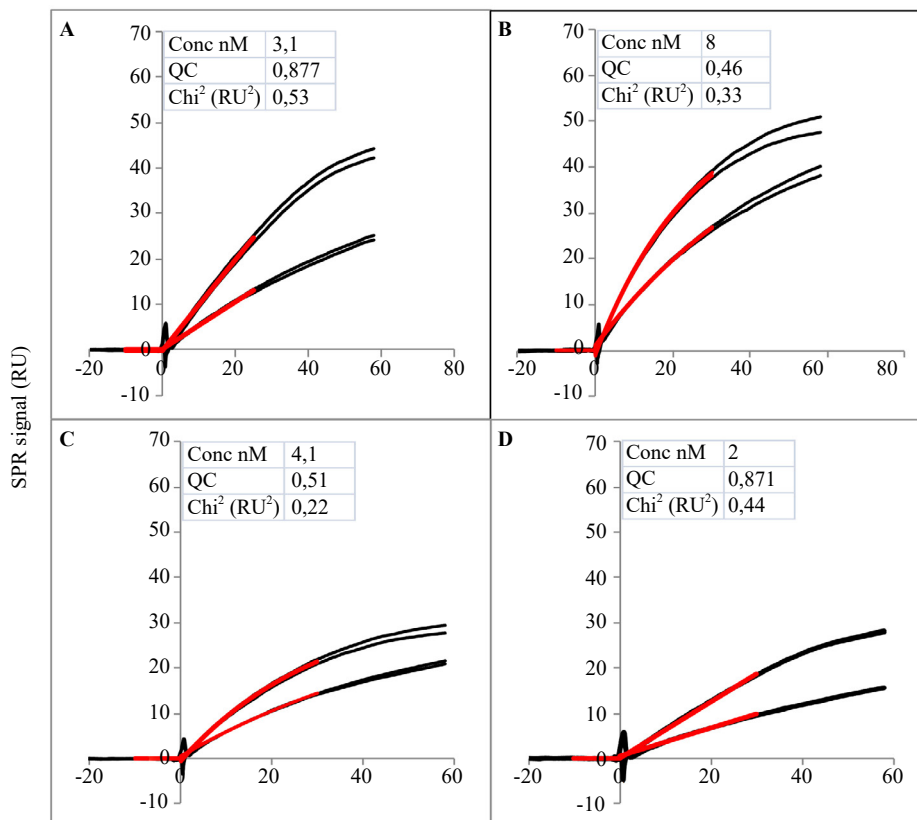
Once it was demonstrated that the mutated VHH kept its general characteristics, particularly regarding antigen recognition, two other factors were rapidly evaluated: quantity and solubility. As stated below (**Table 2**), the amount of each mutated VHH obtained was comprised of between 0.2 and 2.7 mg/mL for the double mutants and the K75PrY, respectively. Because at that stage the goal was not to enhance the production and yield, we did not enter the long optimization process, as we did in other circumstances for antibody production in mammalian cells [33]. Our net result was obtaining 5 mg/L of the double mutant VHH (**dM1**), the most difficult to obtain. We are confident that a minimal amount of 30 to 50 mg/L of culture can be reached once the culture parameters are adequately adjusted and optimized.

Another aspect of the transformation has also to be determined: the solubility. It is clear that the introduction in the VHH sequence of 1 or 2 amino acids possessing either a long alkyl chain or an aromatic moiety as side chains might influence the overall solubility of the mutated VHHs. In fact, as indirectly stated in the following section, no major changes in the behavior of the VHHs were recorded during their manipulation in the SPR experiments. It is nevertheless a parameter that should be taken into account for the use of ncAA.

**Table 2.** Percentage of active anti-HER2 VHH in each batch determined by SPR

VHH	Total protein concentration (mg/ml)	Total protein concentration (M)	Active protein concentration (M)	Ratio of active VHH (%)
WT	7	5.0 E-04	7.8 E-04	155 %
I27AzK	1.8	1.3 E-04	1.0 E-04	80 %
K75PrY	2.7	1.9 E-04	1.9 E-04	100 %
dM1	0.2	1.4 E-05	5.9 E-06	41 %

Protein concentrations were evaluated from the global fitting of SPR. Interaction curves obtained for VHH dilutions ran at two different flowrates in duplicate. According to the availability of the samples, two data sets were generated for VHH-WT, K75PrY, and dM1. Standard error values were lower than 20%.



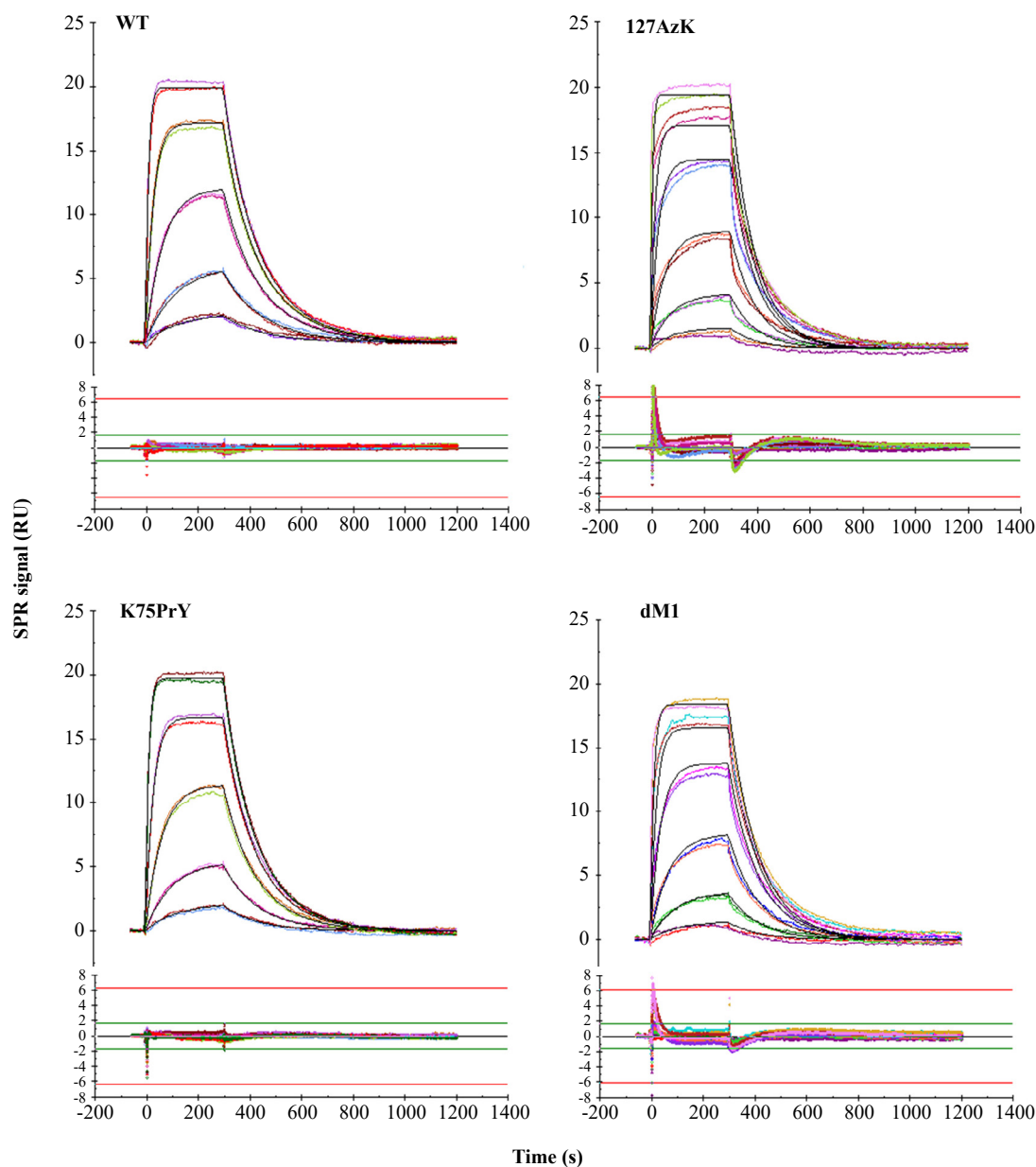
CFCA fits for the binding between immobilized HER2 antigen (5,000 RU) and a VHH dilution [ $\sim 2$  nM (A and D) or 10 nM (B and C)] tested in duplicates at two different flow rates (10 and 80  $\mu\text{L}/\text{min}$ ). The figures show overlay plots of experimental (black) and calculated (red) data. The calculated concentration, the closeness of the fit ( $\chi^2$ ), and the degree of mass transport limitation (QC ratio) are indicated in each plot.

**Figure 6.** CFCA of VHH active concentration. WT (A), I27AzK (B), K75PrY (C), and dM1 (D)

### 3.6.1 Measurements of the VHH–HER2 interactions

The binding parameters of VHH samples were determined with a sensor surface exposing a low level of immobilized HER2 protein (120 RU). According to SPR technical standards, kinetic measurements could be processed after ensuring that the binding rate was not affected by the flow rate (data not shown). The binding profiles were fitted to a simple 1 to 1 interaction model (Figure 7), and the residual plots obtained in global analysis of each binding curves are shown. They are randomly distributed for VHH WT-HER2 and VHH **K75PrY**-HER2 interactions, indicating a good quality of the fits. The evaluated kinetic parameters for VHH WT-HER2 interaction were consistent with the ones previously reported for VHHs produced by *E. coli* [34] ( $k_{\text{on}} = 2.0 \times 10^6 \pm 0.4 \times 10^6 \text{ M}^{-1} \cdot \text{s}^{-1}$ ,  $k_{\text{off}} = 5.6 \times 10^{-3} \pm 0.2 \times 10^{-3} \text{ M}^{-1} \cdot \text{s}^{-1}$ ,  $K_D = 2.8 \pm 0.5 \text{ nM}$ ). VHH WT and the mutant **K75PrY** bind with similar kinetics and affinity to HER2. The data obtained with VHH-**I27AzK** and VHH-**dM1** do not overlay exactly the 1 to 1 model because of a small amount of complexity. This is likely due to the presence of oligomeric VHH molecules (see Figure 2) or conformationally heterogeneous VHH molecules. For the VHH **I27AzK** and **dM1** mutants, the affinities for the immobilized HER2 are about 2.5 to 10 times lower compared to the VHH-WT. The quality of the SPR experiment data may be improved with more homogeneous VHH preparations. The whole set of parameters for these VHH affinities is gathered in Table 3, but the parameters remain in the nM range from 4 to 40 nM, maintaining the affinity of the mutant VHHs for their antigen, HER2, in a restricted range of changes, sensibly similar to what is reported in the literature for WT VHHs in general.





Sensorgrams of the interaction between immobilized HER2 antigen (120 RU) and VHH samples injected in duplicate at different concentrations. The experimental curves (colors) were fitted with a 1:1 Langmuir binding model (black) using BIACORE T200 evaluation software. Residual plots obtained in global analysis of each binding curve are shown.

**Figure 7.** SPR binding profiles of VHH-HER2 interactions

**Table 3.** Binding parameters of anti-HER2 WT VHH and mutants to HER2

VHH	$k_a$ ( $M^{-1}.s^{-1}$ )	$k_d$ ( $s^{-1}$ )	$K_D$ (nM)	$R_{max}$
WT	2.0 E+06	8.4 E-03	4	22
I27AzK	$3 \pm 0.8$ E+05	$1 \pm 0.04$ E-02	$40 \pm 10$	$23 \pm 3.2$
K75PrY	2.8 E+06	8.5 E-03	3	22
dM1	$6 \pm 2$ E+05	$8 \pm 0.4$ E-03	$10 \pm 5$	$20 \pm 0.9$

The binding parameters were globally fitted from experiments run in duplicate. Depending on the availability of the samples, two data sets were generated, and standard error values were calculated from both measurements.

## 4. Discussion

The labeling of VHHs has been reviewed by Barakat et al. [35] and has been successfully used in cancer diagnostic approaches [36-38], but often suffers from the maleimide-based chemical modification of the pure natural VHH by the fluorophore. As presented herein, introducing a chemical handle for alternative and more specific chemical modifications might be a decisive step for the quality of the final fluorescent VHH product and thus an easier tool for VHH's multiple uses. These concepts are thoroughly described and discussed in a recent review [21], in which it is clearly stated that many more experiments in this type of VHH incorporation of non-canonical amino acids will be necessary to delineate the limits of those changes. Indeed, it must be pointed out that those changes not only have a possible impact on the structure of the VHH and thus on its capacity to recognize its target, but that the chemical step(s) necessary to introduce a reporter molecule could also have an impact on the VHH parameters. The hindrance of such reported molecules – DNA, toxin, and fluorophores – might have an impact on the VHH characteristics that must be validated step by step (see also below).

As shown and discussed in our preceding publications [17, 23, 24, 39], VHH might be a step towards “easier-to-use-and-produce” short proteins with therapeutical and imaging (diagnostic) potential. We developed an approach to producing VHH proteins containing ncAA in *E. coli* with specific incorporation of the two ncAAs at the two targeted positions. All proteins were efficiently produced in *E. coli* and purified. This anti-HER2 capacity of these VHHs was maintained despite the modification of up to two amino acids into ncAAs. Those incorporations were quality controlled by LC/MS, and their lack of influence on the parameters of the VHH recognition of their target, HER2, was demonstrated by SPR. Nonetheless, the slight changes in affinity of the mutated VHHs towards HER2 also suggest that such incorporation might also serve to modulate the VHH-antigen binding and potentially the VHH function.

The potential of these molecules is easily understandable, as they combine the formidable protein recognition capacity of antibodies with a size that is about ten times smaller than their antibody counterpart. These features make them an interesting choice to expand the therapeutical arsenal. Indeed, once classical genetic production and characterization were demonstrated and well understood [7], and some VHHs had already entered the pharmacopeia [40, 41], it was interesting to see if further manipulations were possible, like those leading to the possible incorporation of non-canonical amino acids. Those incorporations would permit selective modification of these amino acids by chemical reactions that would preserve the whole VHH and could selectively integrate chemical functions with various properties, such as cytotoxic compounds, fluorophores, or more general pharmacophores bearing an alternative desired effect. These should represent the next steps of VHH pharmacology development for therapeutics [12] as well as for experimental pharmacological use.

The present report was part of a more global program aiming at the use of VHH in different contexts, including the research of specific ways to ultimately target cancerous cells. Considering the timeline at which this program started, it was necessary to address some basic questions about VHHs: their production [24], their total chemical synthesis [23], and even their complexification as potential multitask therapeutical molecules [17].

VHHs have the potential to deliver molecules (“cargos”) at an exquisitely precise cellular location, thanks to their remaining antigen recognition (see also our review on the subject [39]). The “cargos” can be cytotoxic compounds [42, 43], fluorophores or chromophores [35], or radioactive molecules [10, 44]. There are numerous ways in which the cargo is attached or conjugated to the VHHs [45].

These reports led us to explore the possible targeted chemical modification(s) of VHHs. We previously reported the possibility to completely chemically synthesize VHHs, with the concomitant possibility to introduce non-canonical amino acids with chemical functions that would render possible the further incorporation of the “cargo” at dedicated places in the sequence without altering the antigen recognition of the VHH. The remaining steps, for a case-by-case validation, will be 1) to verify that the chemical reaction leading to the introduction of the “cargo” is not harmful to the peptide and 2) to ensure that the ncAA does not alter neither the structure and stability of the VHH nor its antigen recognition. Due to the multiple natures of the cargo, the following validations: chemical, structural, and immunological (molecularly and cellularly) will be required for each chemical entity introduced in the VHH. *A fortiori* with cytotoxic or antiapoptotic compounds that tend to be extremely large molecules [46-48]. An alternative to the direct VHH modification approach is to functionalize, with VHHs, nanoparticles encapsulated with a cytotoxic drug [49].

The present report is meant to be a step prior to the utilization of modified VHHs in diagnostic [50], imaging [9], and research [11] contexts. The possibility of introducing a chemical handle at a specific location of the VHH is

validated, as in the present report. Once this is demonstrated, the next step will be to add to the mutated VHH a chemical such as IRDye700DX for phototherapy [51, 52], a fluorophore [53], a toxin [54], or a cytotoxic compound such as mertansin [55] as those used with alternative methods. Note that for all those described modifications of the VHH, with sometimes very large chemical entities, the basic properties of the final product were unchanged. Any new chemical conjugations will represent the real challenge, as the addition of any compound at these ncAA will change the overall biophysical and pharmacological properties of the final VVH.

After showing that these amino acid(s) do only moderately increase the affinity of the VHH to its target, the alkylation next step will have to be validated, on an alkylating reagent basis (fluorophore, chromophore, radioactive heavy atoms, toxins, cytotoxic agents, etc.), as their influence on the behavior of the VHH will depend on their size, their hindrance, and their biophysical characteristics, and thus each will require *ad hoc* individual validations.

## Funding statement

This work received no external funding.

## Conflict of interest

No author has an actual or perceived conflict of interest with the contents of this article.

## References

- [1] Grabowski H, Cockburn I, Long G. The market for follow-on biologics: How will it evolve? *Health Affairs*. 2006; 25(5): 1291-1301. Available from: <https://doi.org/10.1377/hlthaff.25.5.1291>.
- [2] Rehman FU, Al-Waeel M, Naz SS, Shah KU. Anticancer therapeutics: A brief account on wide refinements. *American Journal of Cancer Research*. 2020; 10(11): 3599-3621.
- [3] Mi J, Xu J, Zhou J, Zhao W, Chen Z, Melenhorst JJ, et al. CAR T-cell immunotherapy: A powerful weapon for fighting hematological B-cell malignancies. *Frontiers of Medicine*. 2021; 15: 783-804. Available from: <https://doi.org/10.1007/s11684-021-0904-z>.
- [4] Barbier AJ, Jiang AY, Zhang P, Wooster R, Anderson DG. The clinical progress of mRNA vaccines and immunotherapies. *Nature Biotechnology*. 2022; 40: 840-854. Available from: <https://doi.org/10.1038/s41587-022-01294-2>.
- [5] Muyldermans S, Atarhouch T, Saldanha J, Barbosa JARG, Hamers R. Sequence and structure of VH domain from naturally occurring camel heavy chain immunoglobulins lacking light chains. *Protein Engineering, Design and Selection*. 1994; 7(9): 1129-1135. Available from: <https://doi.org/10.1093/protein/7.9.1129>.
- [6] Clem LW, Small PA Jr. Phylogeny of immunoglobulin structure and function. I. Immunoglobulins of the lemon shark. *Journal of Experimental Medicine*. 1967; 125(5): 893-920. Available from: <https://doi.org/10.1084/jem.125.5.893>.
- [7] Muyldermans S. Nanobodies: Natural single-domain antibodies. *Annual Review of Biochemistry*. 2013; 82: 775-797. Available from: <https://doi.org/10.1146/annurev-biochem-063011-092449>.
- [8] Muyldermans S. A guide to: Generation and design of nanobodies. *The FEBS Journal*. 2021; 288(7): 2084-2102. Available from: <https://doi.org/10.1111/febs.15515>.
- [9] Harmand TJ, Islam A, Pishesha N, Ploegh HL. Nanobodies as in vivo, non-invasive, imaging agents. *RSC Chemical Biology*. 2021; 2(3): 685-701. Available from: <https://doi.org/10.1039/D1CB00023C>.
- [10] Bao G, Tang M, Zhao J, Zhu X. Nanobody: A promising toolkit for molecular imaging and disease therapy. *EJNMMI Research*. 2021; 11: 6. Available from: <https://doi.org/10.1186/s13550-021-00750-5>.
- [11] Helma J, Cardoso MC, Muyldermans S, Leonhardt H. Nanobodies and recombinant binders in cell biology. *Journal of Cell Biology*. 2015; 209: 633-644. Available from: <https://doi.org/10.1083/jcb.201409074>.
- [12] Debie P, van Quathem J, Hansen I, Bala G, Massa S, Devoogdt N, et al. Effect of dye and conjugation chemistry on the biodistribution profile of near-infrared-labeled nanobodies as tracers for image-guided surgery. *Molecular Pharmaceutics*. 2017; 14(4): 1145-1153. Available from: <https://doi.org/10.1021/acs.molpharmaceut.6b01053>.

- [13] Bannas P, Lenz A, Kunick V, Well L, Fumey W, Rissiek B, et al. Molecular imaging of tumors with nanobodies and antibodies: Timing and dosage are crucial factors for improved in vivo detection. *Contrast Media & Molecular Imaging*. 2015; 10(5): 367-378. Available from: <https://doi.org/10.1002/cmimi.1637>.
- [14] Platonova E, Winterflood CM, Junemann A, Albrecht D, Faix J, Ewers H. Single-molecule microscopy of molecules tagged with GFP or RFP derivatives in mammalian cells using nanobody binders. *Methods*. 2015; 88: 89-97. Available from: <https://doi.org/10.1016/j.ymeth.2015.06.018>.
- [15] Watanabe H, Itagaki F, Shimizu Y, Iikuni S, Ono M. Synthesis and evaluation of a radioiodinated BODIPY derivative as a thiol-labeling agent. *Journal of Labelled Compounds and Radiopharmaceuticals*. 2019; 62: 885-891. Available from: <https://doi.org/10.1002/jlcr.3809>.
- [16] Zhou Z, Zalutsky MR, Vaidyanathan G. Labeling a TCO-functionalized single domain antibody fragment with <sup>18</sup>F via inverse electron demand Diels Alder cycloaddition using a fluoronicotinyl moiety-bearing tetrazine derivative. *Bioorganic & Medicinal Chemistry*. 2020; 28(17): 115634. Available from: <https://doi.org/10.1016/j.bmc.2020.115634>.
- [17] Chabrol E, Fagnen C, Landron S, Marcheteau E, Stojko J, Guenin S-P, et al. Biochemistry, structure, and cellular internalization of a four nanobody-bearing Fc dimer. *Protein Science*. 2021; 30: 1946-1957. Available from: <https://doi.org/10.1002/pro.4147>.
- [18] Krauskopf K, Lang K. Increasing the chemical space of proteins in living cells via genetic code expansion. *Current Opinion in Chemical Biology*. 2020; 58: 112-120. Available from: <https://doi.org/10.1016/j.cbpa.2020.07.012>.
- [19] Quast RB, Fatemi F, Kranendonk M, Margeat E, Truan G. Accurate determination of human CPR conformational equilibrium by smFRET using dual orthogonal noncanonical amino acid labeling. *Chembiochem*. 2019; 20: 659-666. Available from: <https://doi.org/10.1002/cbic.201800607>.
- [20] Smolskaya S, Andreev YA. Site-specific incorporation of unnatural amino acids into Escherichia coli recombinant protein: Methodology development and recent achievement. *Biomolecules*. 2019; 9(7): 255. Available at: <https://doi.org/10.3390/biom9070255>.
- [21] Gettemans J, De Dobbelaer B. Transforming nanobodies into high-precision tools for protein function analysis. *American Journal of Physiology: Cell Physiology*. 2021; 320(2): C195-C215. Available from: <https://doi.org/10.1152/ajpcell.00435.2020>.
- [22] Yong KW, Yuen D, Chen MZ, Johnston APR. Engineering the orientation, density, and flexibility of single-domain antibodies on nanoparticles to improve cell targeting. *ACS Applied Materials & Interfaces*. 2020; 12(5): 5593-5600. Available from: <https://doi.org/10.1021/acsami.9b20993>.
- [23] Hartmann L, Botzanowski T, Galibert M, Jullian M, Chabrol E, Zeder-Lutz G, et al. VHH characterization. Comparison of recombinant with chemically synthesized anti-HER2 VHH. *Protein Science*. 2019; 28: 1865-1879. Available from: <https://doi.org/10.1002/pro.3712>.
- [24] Chabrol E, Stojko J, Nicolas A, Botzanowski T, Fould B, Antoine M, et al. VHH characterization. Recombinant VHHs: Production, characterization and affinity. *Analytical Biochemistry*. 2020; 589: 113491. Available from: <https://doi.org/10.1016/j.ab.2019.113491>.
- [25] Johnsson B, Löfås S, Lindquist G. Immobilization of proteins to a carboxymethyl dextran-modified gold surface for biospecific interaction analysis in surface plasmon resonance sensors. *Analytical Biochemistry*. 1991; 198(2): 268-277. Available from: [https://doi.org/10.1016/0003-2697\(91\)90424-R](https://doi.org/10.1016/0003-2697(91)90424-R).
- [26] Pol E, Roos H, Markey F, Elwinger F, Shaw A, Karlsson R. Evaluation of calibration-free concentration analysis provided by Biacore™ systems. *Analytical Biochemistry*. 2016; 510: 88-97. Available from: <https://doi.org/10.1016/j.ab.2016.07.009>.
- [27] Karlsson R. Biosensor binding data and its applicability to the determination of active concentration. *Biophysical Reviews*. 2016; 8: 347-358. Available from: <https://doi.org/10.1007/s12551-016-0219-5>.
- [28] Myszka DG. Improving biosensor analysis. *Journal of Molecular Recognition*. 1999; 12: 279-284. Available from: [https://doi.org/10.1002/\(SICI\)1099-1352\(199909/10\)12:5<279::AID-JMR473>3.0.CO;2-3](https://doi.org/10.1002/(SICI)1099-1352(199909/10)12:5<279::AID-JMR473>3.0.CO;2-3).
- [29] Myszka DG, Wood SJ, Biere AL. [25] Analysis of fibril elongation using surface plasmon resonance biosensors. *Methods in Enzymology*. 1999; 309: 386-402. Available from: [https://doi.org/10.1016/S0076-6879\(99\)09027-8](https://doi.org/10.1016/S0076-6879(99)09027-8).
- [30] Rigolot V, Biot C, Lion C. To view your biomolecule, click inside the cell. *Angewandte Chemie International Edition*. 2021; 60(43): 23084-23105. Available from: <https://doi.org/10.1002/anie.202101502>.
- [31] Lee KJ, Kang D, Park H-S. Site-specific labeling of proteins using unnatural amino acids. *Molecules and Cells*. 2019; 42(5): 386-396. Available from: <https://doi.org/10.14348/molcells.2019.0078>.
- [32] Bacchi M, Fould B, Jullian M, Kreiter A, Maurras A, Nosjean O, et al. Screening ubiquitin specific protease activities using chemically synthesized ubiquitin and ubiquitinated peptides. *Analytical Biochemistry*. 2017; 519: 57-70. Available from: <https://doi.org/10.1016/j.ab.2016.12.014>.

- [33] Maria S, Bonneau L, Fould B, Ferry G, Boutin JA, Cabanne C, et al. Perfusion process for CHO cell producing monoclonal antibody: Comparison of methods to determine optimum cell specific perfusion rate. *Biochemical Engineering Journal*. 2023; 191: 108779. Available from: <https://doi.org/10.1016/j.bej.2022.108779>.
- [34] Hartmann L, Kugler V, Wagner R. Expression of eukaryotic membrane proteins in *Pichia pastoris*. In: Mus-Veteau I. (ed.) *Heterologous expression of membrane proteins*. New York, USA: Humana Press; 2016. p.143-162. Available from: [https://doi.org/10.1007/978-1-4939-3637-3\\_10](https://doi.org/10.1007/978-1-4939-3637-3_10).
- [35] Barakat S, Berksöz M, Zahedimaram P, Piepoli S, Erman B. Nanobodies as molecular imaging probes. *Free Radical Biology and Medicine*. 2022; 182: 260-275. Available from: <https://doi.org/10.1016/j.freeradbiomed.2022.02.031>.
- [36] Kijanka M, Warnders F-J, El Khattabi M, Hooze ML, van Dam GM, Ntziachristos V, et al. Rapid optical imaging of human breast tumour xenografts using anti-HER2 VHHs site-directly conjugated to IRDye 800CW for image-guided surgery. *European Journal of Nuclear Medicine and Molecular Imaging*. 2013; 40: 1718-1729. Available from: <https://doi.org/10.1007/s00259-013-2471-2>.
- [37] Oliveira S, van Dongen GAMS, Walsum MSV, Roovers RC, Stam JC, Mali W, et al. Rapid visualization of human tumor xenografts through optical imaging with a near-infrared fluorescent anti-epidermal growth factor receptor nanobody. *Molecular Imaging*. 2012; 11(1). Available from: <https://doi.org/10.2310/7290.2011.00025>.
- [38] Fumey W, Koenigsdorf J, Kunick V, Menzel S, Schütze K, Unger M, et al. Nanobodies effectively modulate the enzymatic activity of CD38 and allow specific imaging of CD38<sup>+</sup> tumors in mouse models *in vivo*. *Scientific Reports*. 2017; 7: 14289. Available from: <https://doi.org/10.1038/s41598-017-14112-6>.
- [39] Ferry G, Chabrol E, Boutin JA. Nanobodies in the pharmaceutical industry: Possible trends. *Advances in Nanotechnology*. 2022; 27: 61-82.
- [40] Bhakta S, Crocker LM, Chen Y, Hazen M, Schutten MM, Li D, et al. An anti-GDNF Family Receptor Alpha 1 (GFRA1) antibody-drug conjugate for the treatment of hormone receptor-positive breast cancer. *Molecular Cancer Therapeutics*. 2018; 17(3): 638-649. Available from: <https://doi.org/10.1158/1535-7163.MCT-17-0813>.
- [41] Keam SJ. Ozoralizumab: First approval. *Drugs*. 2023; 83: 87-92. Available from: <https://doi.org/10.1007/s40265-022-01821-0>.
- [42] Huang H, Wu T, Shi H, Wu Y, Yang H, Zhong K, et al. Modular design of nanobody-drug conjugates for targeted-delivery of platinum anticancer drugs with an MRI contrast agent. *Chemical Communications*. 2019; 35: 5175-5178. Available from: <https://doi.org/10.1039/C9CC01391A>.
- [43] Deng C, Xiong J, Gu X, Chen X, Wu S, Wang Z, et al. Novel recombinant immunotoxin of EGFR specific nanobody fused with cucurmosin, construction and antitumor efficiency *in vitro*. *Oncotarget*. 2017; 8: 38568-38580. Available from: <https://doi.org/10.18632/oncotarget.16930>.
- [44] Pruszyński M, Koumariou E, Vaidyanathan G, Revets H, Devoogdt N, Lahoutte T, et al. Improved tumor targeting of anti-HER2 nanobody through N-succinimidyl 4-guanidinomethyl-3-iodobenzoate radiolabeling. *Journal of Nuclear Medicine*. 2014; 55(4): 650-656. Available from: <https://doi.org/10.2967/jnumed.113.127100>.
- [45] Panikar SS, Banu N, Haramati J, del Toro-Arreola S, Leal AL, Salas P. Nanobodies as efficient drug-carriers: Progress and trends in chemotherapy. *Journal of Controlled Release*. 2021; 334: 389-412. Available from: <https://doi.org/10.1016/j.jconrel.2021.05.004>.
- [46] Szlavik Z, Ondi L, Csékei M, Paczal A, Szabó ZB, Radics G, et al. Structure-guided discovery of a selective Mcl-1 inhibitor with cellular activity. *Journal of Medicinal Chemistry*. 2019; 62(15): 6913-6924. Available from: <https://doi.org/10.1021/acs.jmedchem.9b00134>.
- [47] Szlavik Z, Csekei M, Paczal A, Szabo ZB, Sipos S, Radics G, et al. Discovery of S64315, a potent and selective Mcl-1 inhibitor. *Journal of Medicinal Chemistry*. 2020; 63: 13762-13795. Available from: <https://doi.org/10.1021/acs.jmedchem.0c01234>.
- [48] Murray JB, Davidson J, Chen I, Davis B, Dokurno P, Graham CJ, et al. Establishing drug discovery and identification of hit series for the anti-apoptotic proteins, Bcl-2 and Mcl-1. *ACS Omega*. 2019; 4(5): 8892-8906. Available from: <https://doi.org/10.1021/acsomega.9b00611>.
- [49] Pothin E, Lesuisse D, Lafaye P. Brain delivery of single-domain antibodies: A focus on VHH and VNAR. *Pharmaceutics*. 2020; 12(10): 937. Available from: <https://doi.org/10.3390/pharmaceutics12100937>.
- [50] Hoey RJ, Eom H, Horn JR. Structure and development of single domain antibodies as modules for therapeutics and diagnostics. *Experimental Biology and Medicine*. 2019; 244(17): 1568-1576. Available from: <https://doi.org/10.1177/1535370219881129>.
- [51] Mashayekhi V, Xenaki KT, van Bergen en Henegouwen PMP, Oliveira S. Dual targeting of endothelial and cancer cells potentiates *in vitro* nanobody-targeted photodynamic therapy. *Cancers*. 2020; 12(10): 2732. Available from: <https://doi.org/10.3390/cancers12102732>.
- [52] deGroof TWM, Mashayekhi V, Fan TS, Bergkamp ND, Toraño JS, van Senten JR, et al. Nanobody-targeted



- photodynamic therapy selectively kills viral GPCR-expressing glioblastoma cells. *Molecular Pharmaceutics*. 2019; 16(7): 3145-3156. Available from: <https://doi.org/10.1021/acs.molpharmaceut.9b00360>.
- [53] Kijanka MM, van Brussel ASA, van der Wall E, Mali WPTM, van Diest PJ, van Bergen en Henegouwen PMP, et al. Optical imaging of pre-invasive breast cancer with a combination of VHHs targeting CAIX and HER2 increases contrast and facilitates tumour characterization. *EJNMMI Research*. 2016; 6: 14. Available from: <https://doi.org/10.1186/s13550-016-0166-y>.
- [54] Shajari S, Farajollahi MM, Behdani M, Tarighi P. Production and conjugation of truncated recombinant diphtheria toxin to VEGFR-2 specific nanobody and evaluation of its cytotoxic effect on PC-3 cell line. *Molecular Biotechnology*. 2022; 64: 1218-1226. Available from: <https://doi.org/10.1007/s12033-022-00485-1>.
- [55] Henry KA, Nguyen T-D, Baral TN, Hussack G, Raphael S, Arbabi-Ghahroudi M, et al. Biparatopic single-domain antibodies against Axl achieve ultra-high affinity through intramolecular engagement. *Biochemical and Biophysical Research Communications*. 2021; 562: 154-161. Available from: <https://doi.org/10.1016/j.bbrc.2021.05.030>.